



Journal of Ultrafine Grained and Nanostructured Materials

<https://jufgnsm.ut.ac.ir>

Vol. 53, No.2, December 2020, pp. 158-165

Print ISSN: 2423-6845 Online ISSN: 2423-6837

DOI: [10.22059/jufgnsm.2020.02.07](https://doi.org/10.22059/jufgnsm.2020.02.07)

Cryomilling-Assisted Synthesis of Nanostructured Silicon

Elnaz Shahsavar¹, Cyrus Zamani^{*1,2}, Hossein Ahmadi Dermenⁱ¹, Ali Mohammad Hadian¹, Amir Hadian²

¹School of Metallurgy and Materials Engineering, College of Engineering, University of Tehran, Tehran, Iran.

²Empa, Swiss Federal Laboratories for Materials Science & Technology, Laboratory for High Performance Ceramics, 8600, Dübendorf, Switzerland.

Received: 29 October 2020; Accepted: 27 November 2020

* Corresponding author email: c.zamani@ut.ac.ir

ABSTRACT

Rice husk-derived nanostructured silicon is synthesized using a cryogenic milling system. After calcination of rice husk at 700°C, obtained silica was mixed with magnesium powder via cryomilling at -100°C for 1 to 6 hours, followed by a magnesiothermic reduction heat treatment. Electron microscopy results revealed the quality of mixing process with no chemical reaction occurred during milling as confirmed by X-ray diffraction analysis. Prolonged cryomilling not only improved the distribution of the powders but also provided a highly active magnesium powder inside the mixture. As a result, a final product with larger total pore volume and higher surface area was obtained. Finally, cryomilling for 6 hours combined with magnesiothermic in powder form (as compared to pelletized material) resulted in the highest total pore volume of 0.258 cm³.g⁻¹ (corresponding to average pore diameter of 20.42 nm) and specific surface area of 50.44 m².g⁻¹. The average crystallite size of all samples is in the range of 45.57 to 53.28 nm, thus confirming formation of the nanostructured silicon.

Keywords: Rice husk, nanostructured silica, nanostructured silicon, cryomilling, magnesiothermic reduction.

1. Introduction

Nanostructured silicon has found numerous applications in photovoltaics, thermoelectrics, biosensor devices, and lithium-ion batteries [1, 2]. The material can be synthesized through several processes among which, magnesiothermic reduction of rice husk-derived silica is considered as a facile method for the production of battery-grade nanostructured silicon [3]. Azadeh et al. reported a calcination route for rice husk with a 94.6% silica production efficiency[4]. In another work, Chen et al. obtained porous silicon via magnesiothermic reduction and with a specific surface area of 162 m²/g much karger than commercial silicon with a surface area of 20 m²/g [5]. According to Lee et

al., compression of precursors before reduction reaction decreases the initial temperature of exothermic reactions because of better particle contact and more convenient heat transfer [6].

On the other hand, it is now evident that cryomilling enhances the brittleness of ductile powders and improves pulverization efficiency via extensive collision between milling balls and container walls. In addition, low temperature is expected to postpone reactions that may occur during conventional milling at room temperature [7, 8]. Hou et al. investigated the effect of cryomilling on the Al-Fe₂O₃ mixture and concluded that cryomilling reduces particle size in a metal-ceramic system more efficiently as compared to

room temperature milling and also inhibits the reaction between particles during milling [9].

In this work, the effect of cryomilling on pulverization and mixing of magnesium and silica powders and their pelletizing behaviour is investigated.

2. Experimental

Rice husk was purchased from rice fields of Babol, north Iran. Magnesium powder (60-300 μm), hydrochloric acid (37% wt), acetic acid (37% wt), and ethanol (99.6% wt,) were of analytical grade and were used as received.

In the first step, 50 g of rice husk was washed with distilled water followed by soaking in 1M HCl at room temperature for 2 hours to remove impurities and then dried overnight at 100°C. 10 g of acid-washed rice husk was heated up to 700°C with a heating rate of 16°C/min in air atmosphere for 3 hours to remove organic constituents. Finally, 1.8 g of Silica was obtained.

The milling apparatus is shown in fig.1. The system is comprised of a central 350cm³ 316 stainless steel container and two outer containers around it. Liquid nitrogen is purged into the first space while its temperature is controlled using a thermocouple. The second container's air is pumped out using a vacuum pump to minimize heat transfer between the main container and the environment.

A mixture of Silica and magnesium powder (Mg/ SiO₂ Molar ratio:2) and ethanol was added to the milling container. The container sealed under

argon gas and cooled down to -90°C to -100°C using liquid nitrogen with no contact between nitrogen gas and mixture. Milling was performed from 1 to 6 hours with 10mm 316 Stainless steel balls and a Ball to powder ratio (bpr) of 75. Milling conditions are shown in Table.1. After milling, iron impurities were removed using magnets during stirring. For the sake of comparison, two samples were prepared one with hand-mixing and the other with room temperature milling (for 1 hour).

For magnesiothermic reduction, two sets of milled mixtures were prepared. The first set was compressed to a pellet-like shape using a cylindrical die while the second group was used as loose powders with no compression. Samples were heated at 650°C in an argon-filled tube furnace for 1 hour. Reduced samples were stirred in hydrochloric acid and acetic acid aqueous solution (1.25M and 4.38 M, respectively) at 70°C for 4 hours and then washed subsequently to reach a pH of 7. Washed powders were dried at 70°C for 10 hours to obtain nanostructured silicon. These acid leached samples were labeled with an L suffix (L stands for leaching).

Crystal structure of samples were analyzed using X-ray powder diffraction (Rigaku ultima IV) with Cu-K α radiation ($\lambda=1.5404 \text{ \AA}$). Crystallite average size was calculated by the Scherrer equation (Eq. 1)

$$D = (k\lambda)/(\beta \cdot \cos\theta) \quad (1)$$

Where D is the crystallite size (nm), k is shape factor (0.89), λ is the wavelength of Cu- K α

Table 1- Samples preparation conditions

Sample code	RTM75-1	CM75-1	CM75-6	HM
Ball to Powder ratio	75	75	75	No Balls
Preparation method	Room temp. milling	Cryomilling	Cryomilling	Hand-mixed
Milling time (hrs.)	1	1	6	-

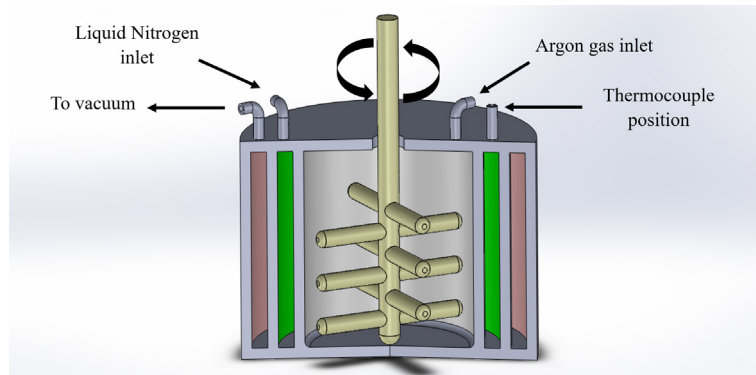


Fig. 1- Schematic image of the cryomilling apparatus.

radiation, θ is the Bragg angles of major diffraction peaks, and β is full width at half maximum (FWHM) of XRD peaks [10] $L=K\lambda/\beta.\cos\theta$, was developed in 1918, to calculate the nano crystallite size (L).

Specific surface area, pore diameters, and their volume were measured using BET/BJH method (BELSORP mini II).

The microstructural analysis was conducted using TESCAN MIRA3 FESEM, equipped with an EDS detector.

Differential scanning calorimetry (DSC) measured using PerkinElmer Simultaneous Thermal Analyzer (STA) 6000 at 700°C with a heating rate of 5 °C/min.

3. Results and discussion

3.1. Synthesis of nanostructured Silica

As shown in Fig. 2. (a&b), rice husk has a rod-like structure, and magnesium powder is composed of ellipsoidal particles with an average size of 68 μ m. Fig. 2.c depicts the morphology of synthesized silica with spherical nanoparticles, 20 to 30 nm in diameter. XRD analysis of the magnesium powder (Fig. 3) reveals that, in addition to magnesium itself (JCPDS 00-035-0821), Mg(OH)₂ (JCPDS 00-007-0239) impurities also exist which may have formed because of humidity. In the case of silica, a wide peak is seen at 22.5°, which is characteristic

of amorphous silica (Fig 3.b). Similar to other researches [4, 11], there is no sign of crystallization after calcination of rice husk.

3.2. Cryomilling

To increase the reduction yield and to avoid the localized heat release, a uniform distribution of precursors is needed. Milling in a wet medium increases particle movement and lowers the friction of the system. Previous studies show that the reaction between powders can occur even at a short milling time at ambient temperature. For instance, the reduction of CuO and MoO₃ in the presence of aluminum starts after 10 minutes of high energy ball milling at room temperature [12]molybdenum-copper/alumina nano composite was synthesized with mechano-chemical method using high energy planetary ball milling. The molybdenum oxide, copper oxide and aluminum powder were used as starting materials and reaction appeared to occur through a rapid combustion reaction process. The evaluation of powder particles after different milling times was studied by X-ray diffraction (XRD). Fig.4 indicates XRD patterns of mixed samples. As expected, no new peak has appeared even after 6 hours of milling, which means that low temperature retards the reactions that may occur during room temperature milling. Silica reduction

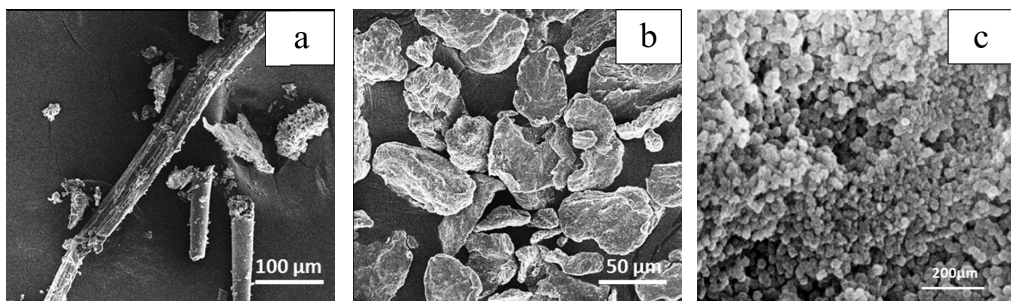


Fig. 2- FE-SEM images of rice husk (a), magnesium powder (b), rice husk-derived silica (c).

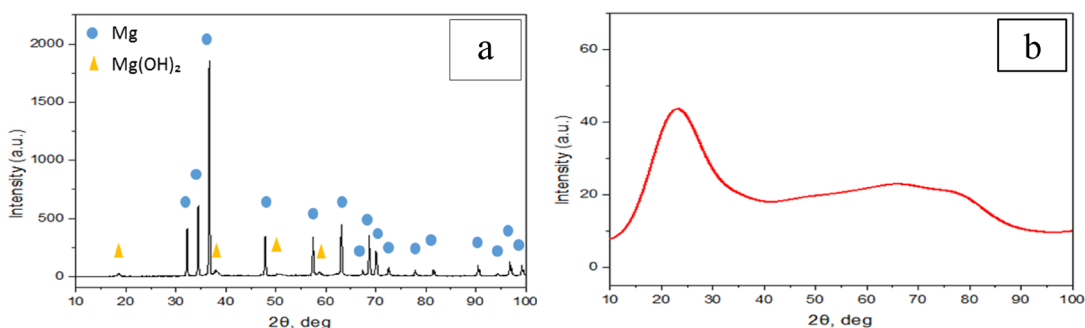


Fig. 3- X-ray diffraction of magnesium powder (a), and rice husk-derived silica(b).

usually starts after a localized temperature increase, but cryomilling causes the heat to dissipate and avoids reaction start. Figs. 5, 6 show the effect of milling condition on the particle size of mixtures. Fig. 5 demonstrates effective size reduction after 6 hours of milling at low temperature. Almost no difference is seen between this sample and the material milled at room temperature for 1h. This is because the energy induced to the mixture is quite low under such conditions as reported elsewhere [13]. Average particle size of RTM75-1, CM75-1, and CM75-6 samples are 5.17 μ m, 4.93 μ m, and 1.11 μ m, respectively. Fig. 6.a-c illustrates elements' distribution in samples. Despite the high amount of iron and chrome impurities, CM75-6 is the best-prepared sample because of its uniform

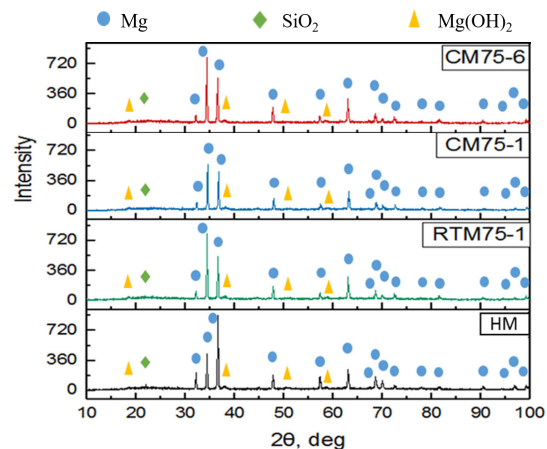


Fig. 4- XRD patterns of mixed samples using different mixing methods.

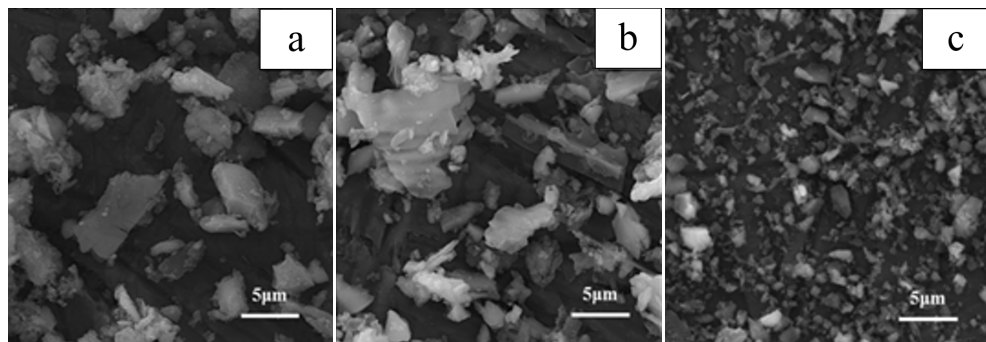


Fig. 5- FE-SEM images of low temperature milled samples, RTM75-1 (a), CM75-1 (b) and CM75-6 (c).

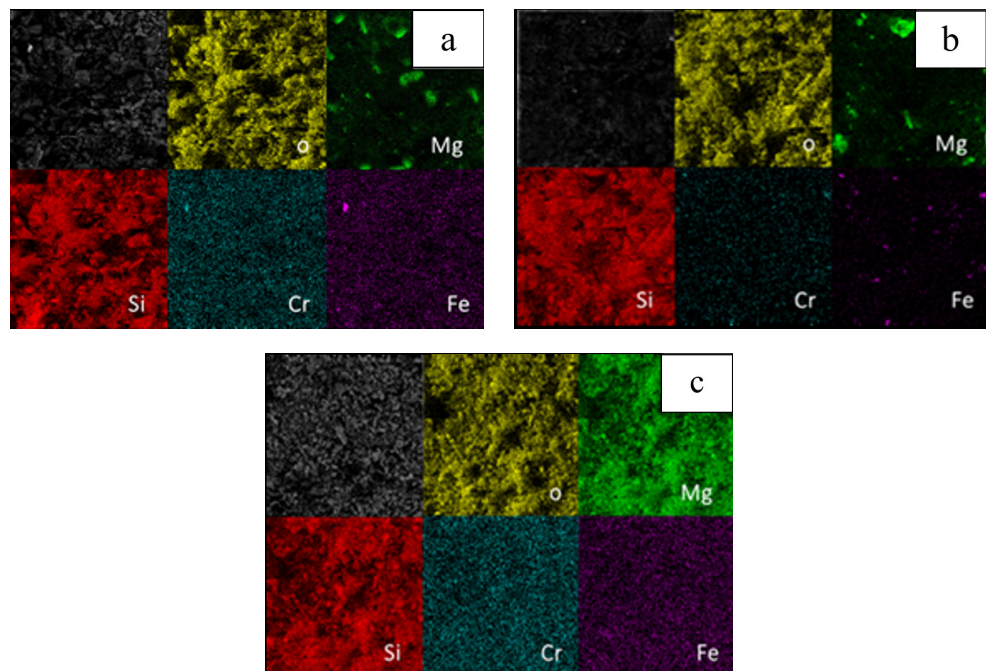


Fig. 6- EDS elemental distribution of milled samples with different milling condition. RTM-1 (a), CM75-1 (b) and CM75-6 (c).

distribution of magnesium and small particle size.

3.3. Magnesiothermic reduction of Silica

To investigate the effect of cryomilling on the magnesiothermic reduction of silica, Differential Scanning Calorimetry (DSC) was conducted on HM and CM75-6 samples. Fig. 7 illustrates the results for these two samples. Silica reduction has an exothermic peak between 550°C and 650°C, according to Eq. 2, but the reduction of silica in the CM75-6 sample starts at lower temperatures.



Smaller particle size and more uniform distribution of magnesium in CM75-6 sample provide more surface area and homogenous release

of heat, which results in a lower energy barrier to start the reactions. Furthermore, the endothermic peak at 320°C is related to the decomposition of Mg(OH)_2 , according to Eq. 3.

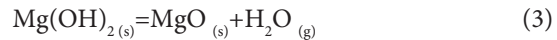


Fig. 8 shows the XRD pattern of acid-washed silicon samples. As shown, 2θ peaks are at 28.4°, 47.4°, 56.1°, 69.2°, 76.4°, 88.1° and 95° matching with JCPDS 00-027-1402 card and related to (111), (220), (311), (400), (331), (422) and (511) crystallographic planes, respectively. Results show the existence of the Mg_2SiO_4 impurity phase in samples. This phase forms due to a lack of magnesium during the reduction process and cannot be removed during acid washing in HCl/

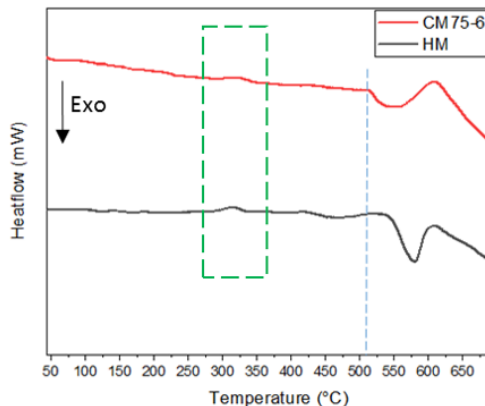


Fig. 7- Differential scanning calorimetry of samples prepared via hand-mixing and 6 hours of cryomilling.

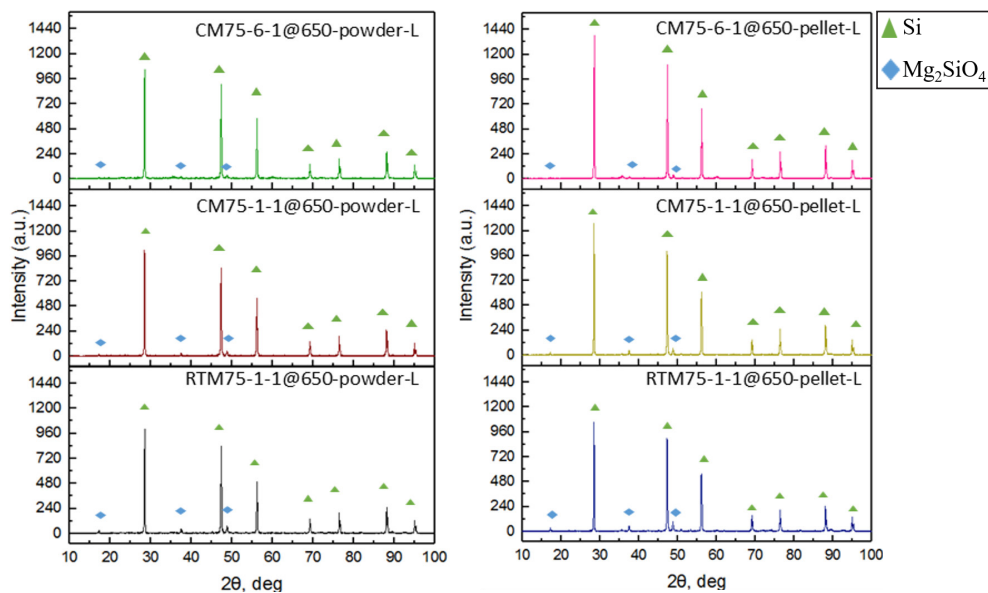


Fig. 8- XRD patterns of final silicon products reduced in powder and pellet format.

CH_3COOH solution [2, 5]. Longer milling time results in a lower amount of Mg_2SiO_4 phase because of smaller particle size and a more uniform presence of magnesium throughout samples. Introducing additional magnesium to the system during reduction can avoid the formation of Mg_2SiO_4 and improves final product purity. Table. 2 demonstrates the crystallite size of silicon in all samples calculated using the Scherrer equation (Eq. 1). All samples contain an average crystallite size of less than 100nm that confirms the production of

nanostructured silicon.

Fig. 9 illustrates the BET isotherms of the samples revealing type IV behavior which is indicative of the presence of nanopores. As shown in table. 3, 6 hours of milling and subsequent reduction of powder mixture results in $50.44 \text{ m}^2/\text{g}$ surface area, which is the most among all samples. Hysteresis loop of adsorption/desorption isotherms, confirms that the structure is mesoporous according to IUPAC classification [5]. Fig. 10 shows BJH pore size and pore distribution in silicon samples.

Table 2- Average crystallite size of final silicon samples

SAMPLE	AVG. CRYSTALLITE SIZE (nm)
RTM75-1-1@650-pellet-L	48.24
CM75-1-1@650-pellet-L	53.28
CM75-6-1@650-pellet-L	48.25
RTM75-1-1@650-powder-L	45.57
CM75-1-1@650-powder-L	48.24
CM75-6-1@650-powder-L	48.25

Table 3- BET/BJH results of silicon samples

Samples	Specific Surface area (m^2/g^{-1})	Cumulative pore volume ($\text{cm}^3/\text{g}^{-1}$)	Pore diameter (nm)
CM75-1-1@650-pellet-L	14.12	0.063	17.72
CM75-1-1@650-powder-L	26.60	0.151	22.64
CM75-6-1@650-pellet-L	34.74	0.170	19.54
CM75-6-1@650-powder-L	50.44	0.258	20.42

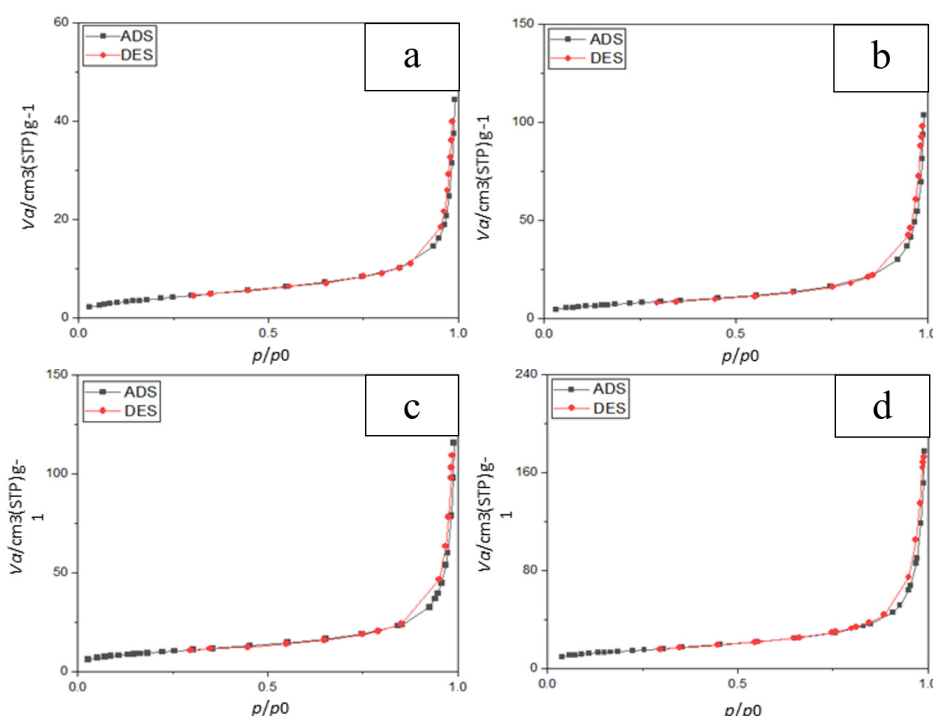


Fig. 9- Isoothermal Adsorption/Desorption of samples: CM75-1-1@650-pellet-L (a), CM75-1-1@650-powder-L (b), CM75-6-1@650-pellet-L (c) and CM75-6-1@650-powder-L (d).

Results disclose a uniform pore size. Furthermore, increasing the milling time and using the loose powdered mixture increases the volume of pores with less than 5 nm in diameter. These findings confirm the efficacy of the employed procedure

as compared to previous results [4, 6, 14]. As a comparison to Azadeh et al., larger surface area with more uniform pore size is obtained in this work. The synthesized porous nanostructured silicon has great potential in electronic applications, especially

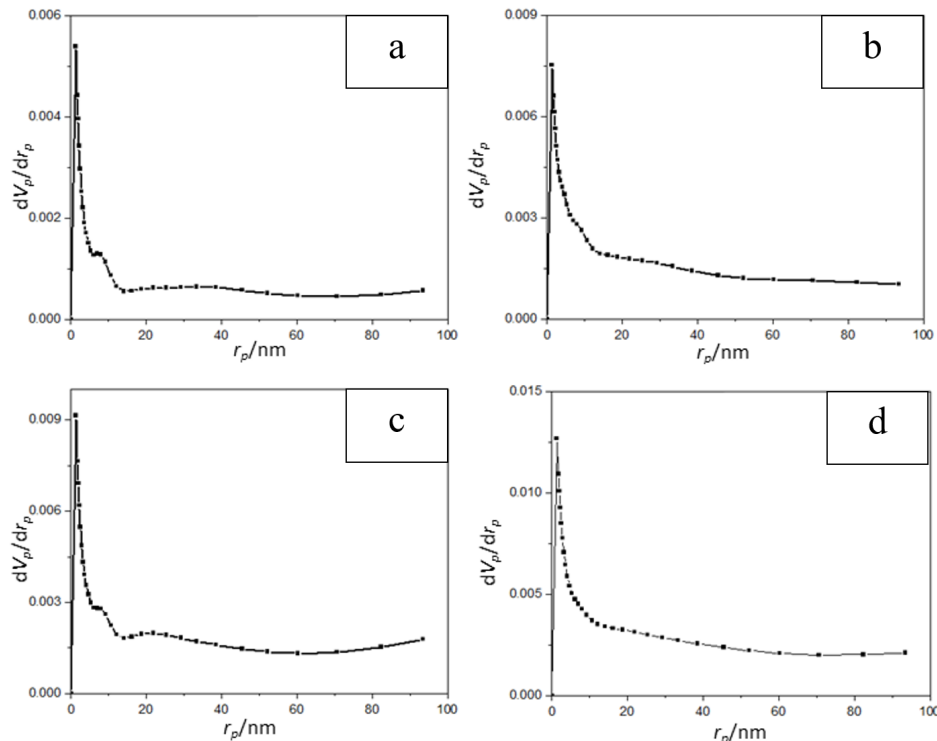


Fig. 10- Pore size distribution of samples: CM75-1-1@650-pellet-L(a), CM75-1-1@650-powder-L (b), CM75-6-1@650-pellet-L (c) and CM75-6-1@650-powder-L (d).

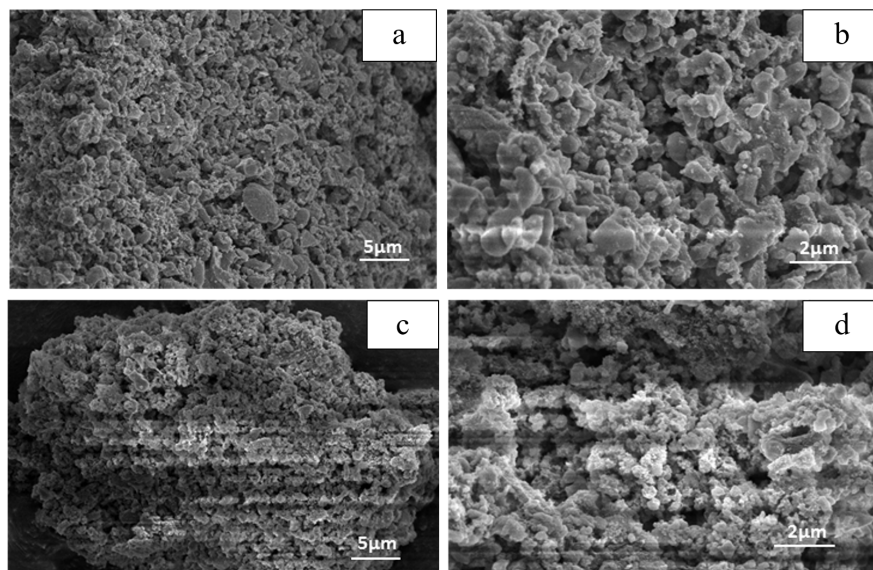


Fig. 11- FE-SEM images of final silicon products at two different magnifications. CM75-1-1@650-powder-L sample (a, b) and CM75-6-1@650-powder-L sample (c, d).

for lithium-ion batteries [15]. Fig. 11 reveals the microstructure of CM75-6-1@650-powder-L and CM75-1-1@650-powder-L samples composed of a matrix that maintains its porous structure similar to its silica source.

4. Conclusion

Nanostructured silicon was synthesized via cryomilling-assisted magnesiothermic reduction. Even after 6 hours of milling at low temperatures, no reaction occurred between precursors, but particle size was reduced significantly. Samples with no compression before magnesiothermic reduction showed larger specific surface area and more uniform distribution of pores less than 5nm in size.

References

1. Won CW, Nersisyan HH, Won HI. Solar-grade silicon powder prepared by combining combustion synthesis with hydrometallurgy. *Solar Energy Materials and Solar Cells*. 2011;95(2):745-50.
2. Shi L, Wang W, Wang A, Yuan K, Yang Y. Understanding the impact mechanism of the thermal effect on the porous silicon anode material preparation via magnesiothermic reduction. *Journal of Alloys and Compounds*. 2016;661:27-37.
3. Kumar S, Sangwan P, Dhankhar RM, Bidra S. Utilization of rice husk and their ash: A review. *Res. J. Chem. Env. Sci*. 2013 Dec;1(5):126-9.
4. Azadeh M, Zamani C, Ataie A, Morante JR. Three-dimensional rice husk-originated mesoporous silicon and its electrical properties. *Materials Today Communications*. 2018;14:141-50.
5. Chen W, Fan Z, Dhanabalan A, Chen C, Wang C. Mesoporous Silicon Anodes Prepared by Magnesiothermic Reduction for Lithium Ion Batteries. *Journal of The Electrochemical Society*. 2011;158(9):A1055.
6. Lee HI, Son SH, Kook JW, Kim HJ, Choi JW, Joo JH, et al. Effect of Pelletizing and Temperature in Silicon Production Using Magnesiothermic Reduction. *JOURNAL OF CHEMICAL ENGINEERING OF JAPAN*. 2018;51(9):794-9.
7. Shi Z-c, Zhang Z-d, Guo J-y, Gao M, Qi X-g, Bi J-q, et al. Magnetic multiresonance behavior of Fe@Al₂O₃ nanoembedments and microstructural evolution during mechanosynthesis. *Journal of Alloys and Compounds*. 2011;509(18):5600-3.
8. Witkin DB, Lavernia EJ. Synthesis and mechanical behavior of nanostructured materials via cryomilling. *Progress in Materials Science*. 2006;51(1):1-60.
9. Hou Q, Shi ZC, Fan RH, Ju LC. Cryomilling and Characterization of Metal/Ceramic Powders. *Key Engineering Materials*. 2012;512-515:127-31.
10. Monshi A, Foroughi MR, Monshi MR. Modified Scherrer Equation to Estimate More Accurately Nano-Crystallite Size Using XRD. *World Journal of Nano Science and Engineering*. 2012;02(03):154-60.
11. Ikram N, Akhter M. X-ray diffraction analysis of silicon prepared from rice husk ash. *Journal of Materials Science*. 1988;23(7):2379-81.
12. Morady S, Talafi Noghani M, Saghafi Yazdi M. Effect of processing parameters on the mechano-chemical synthesis of nano crystalline Mo-Cu/Al₂O₃ composite. *Journal of Ultrafine Grained and Nanostructured Materials*. 2018 Jun 1;51(1):13-9.
13. Setoudeh N, Zamani C, Sajjadnejad M. Mechanochemical synthesis of nanostructured MgXNi_{1-X}O compound by Mg-NiO mixture. *Journal of Ultrafine Grained and Nanostructured Materials*. 2017 Jun 1;50(1):51-9.
14. Cho WC, Kim HJ, Lee HI, Seo MW, Ra HW, Yoon SJ, et al. 5L-Scale Magnesio-Milling Reduction of Nanostructured SiO₂ for High Capacity Silicon Anodes in Lithium-Ion Batteries. *Nano Letters*. 2016;16(11):7261-9.
15. Gao P, Tang H, Xing A, Bao Z. Porous silicon from the magnesiothermic reaction as a high-performance anode material for lithium ion battery applications. *Electrochimica Acta*. 2017;228:545-52.